

Article

Preparation and Phase Change Performance of Graphene Oxide and Silica Composite $\text{Na}_2\text{SO}_4 \cdot 10\text{H}_2\text{O}$ Phase Change Materials (PCMs) as Thermal Energy Storage Materials

Wen Tao ¹, Xiangfa Kong ¹, Anyang Bao ¹, Chuangang Fan ¹ and Yi Zhang ^{1,2,*}

¹ School of Material Science and Engineering, Anhui University of Technology, Anhui 243002, China; wentaowz@sina.com (W.T.); kongxiangfa6@sina.com (X.K.); baoay1999@163.com (A.B.); chgfan@ahut.edu.cn (C.F.)

² Key Laboratory of Green Fabrication and Surface Technology of Advanced Metal Materials (Anhui University of Technology), Ministry of Education, Anhui 243002, China

* Correspondence: zhy1987@ahut.edu.cn

Received: 16 October 2020; Accepted: 12 November 2020; Published: 17 November 2020



Abstract: In this study, a novel nucleating agent composed of graphene oxide (GO) and silicon dioxide (SiO_2) (GO– SiO_2) is developed. GO is used as a skeleton material through which SiO_2 nanomaterials are absorbed and subsequently incorporated into $\text{Na}_2\text{SO}_4 \cdot 10\text{H}_2\text{O}$ phase change materials (PCMs). Furthermore, this study examines the phase change performance of the composite $\text{Na}_2\text{SO}_4 \cdot 10\text{H}_2\text{O}$ materials. Fourier-transform infrared (FTIR) spectra confirmed the physical combination of GO with a SiO_2 nanoparticles. Scanning electron microscope (SEM) results showed that the GO– SiO_2 composite exhibited a layered structure and excellent dispersibility. The GO– SiO_2 composite $\text{Na}_2\text{SO}_4 \cdot 10\text{H}_2\text{O}$ PCMs displayed a low level of supercooling, i.e., about 1.2 °C with the addition of GO– SiO_2 at 2.45 wt%. This was because the synergistic relation of the GO and the high dispersion SiO_2 , imparted more nucleation sites for $\text{Na}_2\text{SO}_4 \cdot 10\text{H}_2\text{O}$. Additionally, the prepared PCMs achieved high phase change latent heat and thermal conductivity, even under these conditions. The results show that the GO– SiO_2 in the $\text{Na}_2\text{SO}_4 \cdot 10\text{H}_2\text{O}$ exhibited advantageous application prospects for the improvement of the thermal performance of hydrate salts.

Keywords: graphene oxide; phase change materials; inorganic hydrate salt; supercooling; thermal energy storage

1. Introduction

Phase change materials (PCMs) are a kind of thermal energy storage material that can provide a high density of heat storage within a small temperature range, i.e., nearly that of the phase change temperature. This characteristic of PCMs makes them suitable for a wide range of applications in solar energy production, building energy conservation, refrigeration logistics, power systems, waste heat recovery, heating and air conditioning, household appliances and so on [1,2]. Inorganic hydrate salts are a kind of PCM that feature characteristics including high phase change latent heat, nonflammability, low cost and high thermal conductivity [3,4]. Compared with organic PCMs, inorganic hydrated salts have demonstrated many potential applications in the field of thermal energy storage [5,6]. However, there are also problems with inorganic hydrate salts, notably their phase separation and level of supercooling, which have become the key issues restricting the application of these kinds of materials [7,8].

The addition of a nucleating agent is an effective way to overcome the low degree of supercooling of inorganic hydrate salts [9,10]. The adsorption of inorganic hydrate salts into porous materials can also reduce the degree of supercooling [11–13]. $\text{Na}_4\text{P}_2\text{O}_7 \cdot 10\text{H}_2\text{O}$ can be used as a nucleating agent to reduce the required degree of supercooling of some hydrate salts [14], while other materials, like $\text{SrCl}_2 \cdot 6\text{H}_2\text{O}$, can be used as nucleating agents of $\text{CaCl}_2 \cdot 6\text{H}_2\text{O}$ due to the common crystal structure of the two salts [15]. Liu et al. [16] experimented with $\text{Na}_2\text{B}_4\text{O}_7 \cdot 10\text{H}_2\text{O}$, using nano- Al_2O_3 as a nucleating core; the results showed that nano- Al_2O_3 acted as nucleating core, and that the supercooling degree could be effectively reduced from 7.8 to 1.6 °C. Expanded graphite (EG) is a kind of carrier material with a porous structure; the adsorption of hydrate salts into the inner space of EG could prevent the leakage of PCMs in the phase change process. Xiao et al. [17] inserted $\text{Ba}(\text{OH})_2 \cdot 8\text{H}_2\text{O}$ into EG; their results showed that the supercooling degree of $\text{Ba}(\text{OH})_2 \cdot 8\text{H}_2\text{O}$ can be reduced from 13 to 2.4 °C. Liu et al. [18] used bentonite as a supporting material of $\text{CH}_3\text{COONa} \cdot 3\text{H}_2\text{O}$, finding it to be helpful in solving the leakage problems of $\text{CH}_3\text{COONa} \cdot 3\text{H}_2\text{O}$ PCMs.

The addition of nanoparticles is not only effective in improving the thermal performance of PCMs; supercooling problems can also be solved in this fashion [19–21]. As a kind of supporting material, nano- SiO_2 presents a porous structure with massive mesoporosity in its inner space, such that PCMs can be well adsorbed therein [22]. Peng et al. [23] used fumed SiO_2 as a nucleating agent; their results showed that the supercooling degree of disodium hydrogen phosphate dodecahydrate ($\text{Na}_2\text{HPO}_4 \cdot 12\text{H}_2\text{O}$) could be reduced from 14.4 to 4.1 °C when 2 wt% of fumed SiO_2 was added. As a kind of two-dimensional nanomaterial, graphene oxide (GO) has been proven to be effective in improving the thermal properties of PCMs. Xu et al. [24] used $\text{SrCl}_2 \cdot 6\text{H}_2\text{O}$ and GO as nucleating agents to reduce the supercooling degree of $\text{CaCl}_2 \cdot 6\text{H}_2\text{O}$, and found that a percentage reduction in supercooling of about 99.2% could be achieved when 0.8 wt% $\text{SrCl}_2 \cdot 6\text{H}_2\text{O}$ and 0.02 wt% GO were admixed. Xia et al. [25] prepared poly(ethylene glycol) (PEG) using GO nanosheets; their results showed that PEG homogeneously intercalated into GO to form composite PCMs with a lamellar structure, resulting in highly thermally conductive and reliable PCMs.

As a kind of commonly used inorganic hydrate salt, sodium sulfate decahydrate ($\text{Na}_2\text{SO}_4 \cdot 10\text{H}_2\text{O}$) possess a phase change temperature of about 32.4 °C and a phase change latent heat of about 254 J/g. This approximate phase change temperature makes it a promising material for energy storage in buildings. However, the supercooling and phase separation of $\text{Na}_2\text{SO}_4 \cdot 10\text{H}_2\text{O}$ also present problems that limit its practical applications [26]. The high dispersibility of SiO_2 nanoparticles is beneficial for the reduction of the degree of supercooling when combined with $\text{Na}_2\text{SO}_4 \cdot 10\text{H}_2\text{O}$ PCMs. GO also exhibits high compatibility with $\text{Na}_2\text{SO}_4 \cdot 10\text{H}_2\text{O}$ PCMs and good thermal conductivity; this is the trend observed in the development of the nanomaterials that are used in inorganic hydrate salts. Nano-nucleating agents must have a high specific surface area to ensure the dispersal of nanomaterials in hydrate salts, and the hydrate salts should have a better phase change energy storage performance when the nanomaterials are incorporated. Currently, there is no research focusing on the nucleating agent composed of SiO_2 and GO and its composite in the hydrate salts. In this study, in order to investigate the nucleating effect of nanoparticles in $\text{Na}_2\text{SO}_4 \cdot 10\text{H}_2\text{O}$, SiO_2 nanoparticles were synthesized through the sol-gel method. Through the composition of GO with the prepared nano- SiO_2 , GO- SiO_2 composites were developed. Their chemical structure, micromorphology and specific surface area were experimentally studied. Also studied was the influence of GO- SiO_2 on the supercooling degree, crystallization behavior, phase change performance and thermal conductivity of $\text{Na}_2\text{SO}_4 \cdot 10\text{H}_2\text{O}$.

2. Materials and Methods

Sodium sulfate decahydrate ($\text{Na}_2\text{SO}_4 \cdot 10\text{H}_2\text{O}$, SSD, analytical grade) was used as the PCM, supplied by Aladdin Chemical Reagent Co., Ltd. (Shanghai, China). Tetraethoxysilane (TEOS, analytical grade) provided by Sinopharm Chemical Reagent Co., Ltd (Shanghai, China), was used as silica precursor. Formamide (analytical grade), supplied by Sinopharm Chemical Reagent Co., Ltd. (Shanghai, China),

was used as organic solvent. Graphene oxide (GO) aqueous dispersion with a solids content of 7.5 g/L was supplied by Jiangnan Graphene Research Institute (Changzhou, China).

SiO₂ nanoparticles were synthesized under standard conditions using formamide solution as a solvent and TEOS as a silica precursor [27]. A certain amount of TEOS was mixed in formamide and stirred in a water bath at about 35 °C. NH₃·H₂O (28 wt%) was added and the pH value of the solution was adjusted to 11. The mixture was stirred for 24 h, filtered and dried to obtain the SiO₂ nanoparticles. The prepared SiO₂ and GO were mixed and ultrasonically dispersed for 2 h; then, the mixture was filtered and dried to obtain the GO–SiO₂ composites. Na₂SO₄·10H₂O and GO–SiO₂ were mixed and magnetically stirred at 45 °C for 0.5 h to obtain the composite PCMs. The mix proportions of the GO–SiO₂ composites and the composite PCMs are shown in Table 1.

Table 1. Mix composition of the GO–SiO₂ composites and the composite phase change materials (PCMs).

Samples	GO/ml	SiO ₂ /g	Na ₂ SO ₄ ·10H ₂ O/g
GO–SiO ₂ (GS-1)	20	2	-
GO–SiO ₂ (GS-2)	40	2	-
GO–SiO ₂ (GS-3)	60	2	-
S-PCMs	-	2	100
GS-PCMs-1	20	2	100
GS-PCMs-2	40	2	100
GS-PCMs-3	60	2	100

The chemical structures of the samples were obtained by Fourier-transform infrared spectroscopy (FTIR, Nicolet 6700, Thermo Scientific, Waltham, MA, USA) with KBr pellets with a wavenumber of 4000 to 400 cm⁻¹ and a scanning speed of 10 cm⁻¹/s. The nitrogen adsorption–desorption isotherms of the prepared SiO₂ and GO–SiO₂ composites were determined by a pore size analyzer (Micromeritics, Asap2460, Norcross, GA, USA). The crystalline behavior of the composite PCMs was characterized by means of X-ray diffraction using an automated X-ray powder diffractometer (XRD, D8 Advance, Bruker, Leipzig, Sachsen, Germany) with CuKα radiation (λ = 1.5418 Å). The surface morphologies of the composite PCMs were observed using a field emission scanning electron microscope (FESEM; FEI, NANO SEM430, Hillsboro, OR, USA). The microstructures of the composite PCMs were detected by transmission electron microscopy (TEM, JEOLJEM-2100, Akishima, Tokyo, Japan) with an accelerating voltage of 200 kV. The phase change behavior of the samples was determined using a differential scanning calorimeter (DSC; Netzsch 200f3, Selbu, Bayern, Germany) in the range of 0 to 60 °C at a heating or cooling rate of 5 °C/min under nitrogen atmosphere.

The supercooling degrees of the samples (S-PCMs, GS-PCMs-1, GS-PCMs-2 and GS-PCMs-3) were tested using a multichannel temperature measuring instrument equipped with a computer, T-type thermocouple and thermostatic water bath. A 30 mL test tube filled with a 30 g sample was put into the thermostatic water bath and heated to about 45 °C; then, the sample was cooled from 45 to 10 °C. The temperature variations of the samples during the process were recorded to obtain the step cooling curves.

The thermal conductivity of the composite PCMs was measured by means of a hot disk thermal conductivity instrument (DRE-2C, Xiangtan Xiangyi Instrument Co., Ltd., Xiangtan, China) based on the transient plane source method and using a probe with a diameter of about 20 mm. Before the test, the probe was placed between two slabs of each sample and compacted. The thickness of each sample was not less than 10 mm, and each sample was tested three times to obtain the average value. The thermal conductivity λ was calculated as follows:

$$\lambda = \alpha \cdot c \cdot \rho$$

where α represents the thermal diffusivity of a sample; c represents the specific heat capacity of a sample; and ρ indicates the density of a sample.

3. Results

3.1. Chemical Structure

The FTIR spectra of SiO₂, GO and GO–SiO₂ are shown in Figure 1. In the spectrum for SiO₂, the characteristic wide bands at 3000 cm^{−1} and 3700 cm^{−1} correspond to the stretching vibrations of –O–H, and the peak at 1640 cm^{−1} corresponds to the vibrations of H–O–H. The absorption peaks at 1051 cm^{−1} refer to the asymmetrical vibrations of Si–O–Si, while the peaks at 787 cm^{−1} and 451 cm^{−1} refer to the symmetrical vibrations of Si–O–Si. In the spectrum for GO, the bands at 3431 cm^{−1} are associated with the O–H stretching vibrations, and the peaks at 1640 cm^{−1} represent the bending vibrations of C–OH. The characteristic absorption peak at 1115 cm^{−1} corresponds to the C–O–C stretching vibrations. The results show that the oxygen-containing groups of GO are mainly hydroxyl(–OH), carboxyl(–COOH) and epoxy groups(C–O–C). The absorption peaks of SiO₂ and GO can be clearly seen from the spectrum of the prepared GO–SiO₂. No other new absorption peaks were present for the spectrum of GO–SiO₂, which shows that there was no chemical reaction between the GO and SiO₂ nanoparticles.

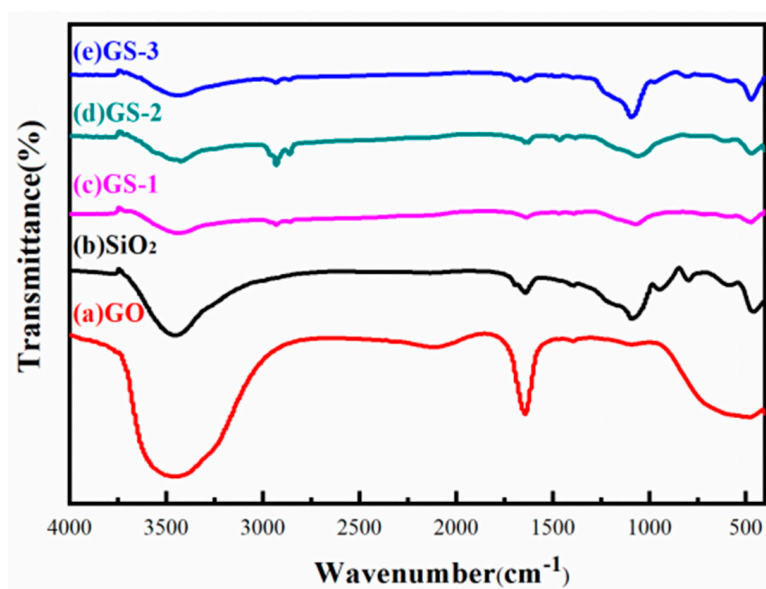


Figure 1. Fourier-transform infrared (FTIR) spectra of GO, SiO₂, GS-1, GS-2 and GS-3.

3.2. Micromorphology and Specific Surface Area Analysis

The micromorphologies of the SiO₂ and GO–SiO₂ composites were observed by scanning electron microscope (SEM). As shown in Figure 2a, the spherical shape of SiO₂ nanoparticles was easily to agglomerate together, with an average particle size of about 200 nm. In Figure 2b–d, showing the GO–SiO₂ composites, the nanosheet structure of GO on which the SiO₂ nanoparticles were absorbed can be clearly seen. As the amount of GO in the GO–SiO₂ composites increased, the adsorption amount of the SiO₂ nanoparticles obviously also increased (Figure 2d), indicating the good compatibility between the GO and the SiO₂ nanoparticles [28,29]. Compared with the synthesized SiO₂ nanoparticles, with the intercalation of GO, the agglomeration degree of the SiO₂ nanoparticles was obviously reduced, while the hybrid network structure of GO–SiO₂ increased the contact surface with the hydrate salts, which is helpful for the crystallization and nucleation of inorganic hydrate salts.

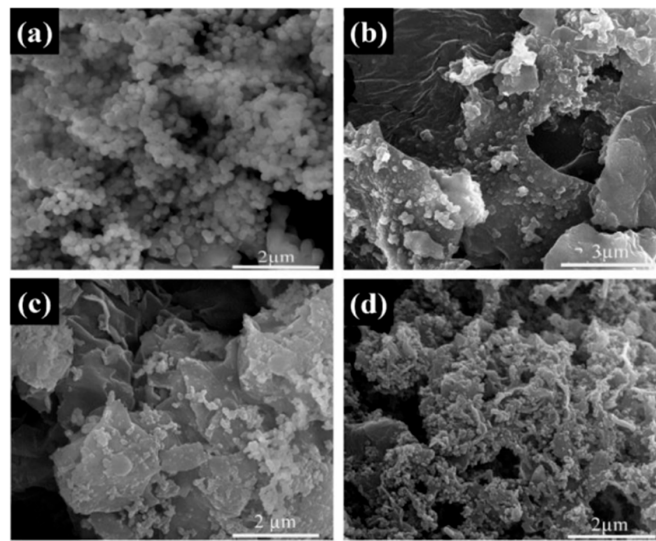


Figure 2. Scanning electron microscope (SEM) images of (a) SiO₂, (b) GS-1, (c) GS-2, (d) GS-3.

The nitrogen adsorption–desorption isotherms of SiO₂ and GO–SiO₂ are shown in Figure 3. The SiO₂ nanoparticles presented a small specific surface area of about 27.53 m²/g. With the addition of GO, the specific surface areas of GS-1, GS-2 and GS-3 were increased to about 67.21 m²/g, 89.30 m²/g and 437.39 m²/g, respectively. A typical type IV isotherm with a hysteresis loop characteristic of relative pressure (P/P_0) higher than 0.8 was observed, and it can be noted that the formation of the pore structure was caused by the accumulation of the nanoparticles. As the amount of GO increased, more and more pores were formed by the accumulation of the nanoparticles, meaning that the adsorption performance of GO–SiO₂ was improved and the hydrate salts could be well adsorbed in the inner space of GO–SiO₂.

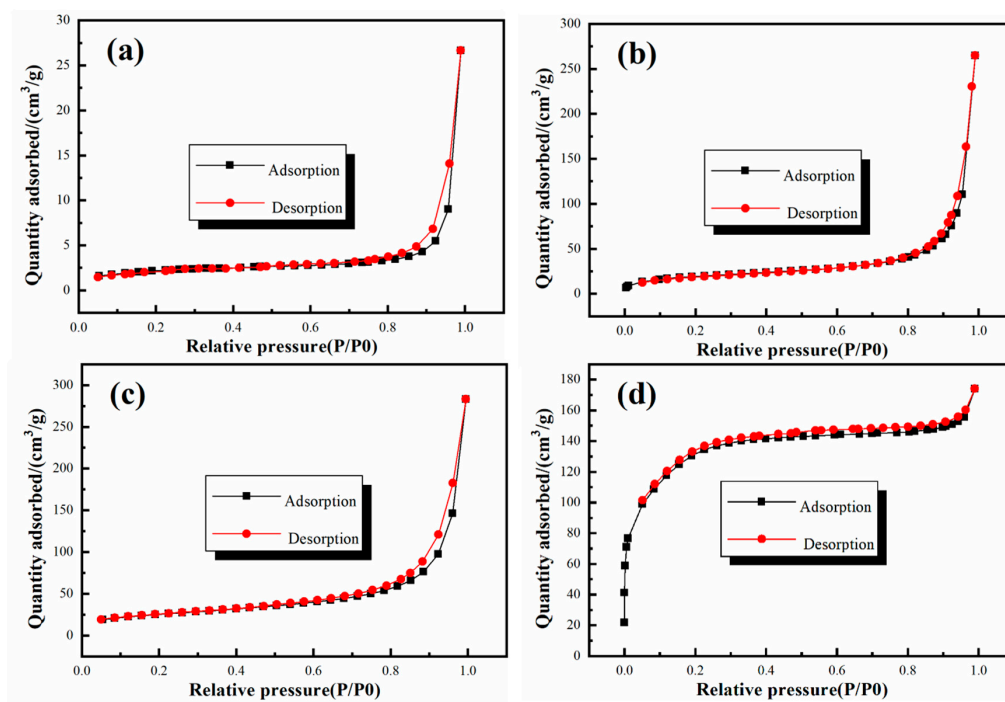


Figure 3. Nitrogen adsorption–desorption isotherms of (a) SiO₂, (b) GS-1, (c) GS-2, (d) GS-3.

3.3. Supercooling Degrees of the $\text{Na}_2\text{SO}_4 \cdot 10\text{H}_2\text{O}$ Composites

The step cooling curves of the pure $\text{Na}_2\text{SO}_4 \cdot 10\text{H}_2\text{O}$, S-PCMs and GS-PCMs are shown in Figure 4. The supercooling degree of the $\text{Na}_2\text{SO}_4 \cdot 10\text{H}_2\text{O}$ was reduced from 10.2 to 3.7 °C when SiO_2 was added. SiO_2 acted as the nucleating core, and the heterogeneous nucleation effect promoted the crystallization of the hydrate salts. For the GO- $\text{SiO}_2/\text{Na}_2\text{SO}_4 \cdot 10\text{H}_2\text{O}$ composites, the addition of GO further reduced the supercooling degree of the hydrate salts; with an increased amount of GO, supercooling degrees of about 3.3 °C, 1.9 °C and 1.2 °C were achieved for GS-PCMs-1, GS-PCMs-2 and GS-PCMs-3, respectively. The results show that the nucleation effect of GO- SiO_2 was further enhanced with the introduction of GO. The increased surface area of GO- SiO_2 provided a larger nucleation site for the hydrate salts, such that the crystallization of the $\text{Na}_2\text{SO}_4 \cdot 10\text{H}_2\text{O}$ could be induced at a lower supercooling degree.

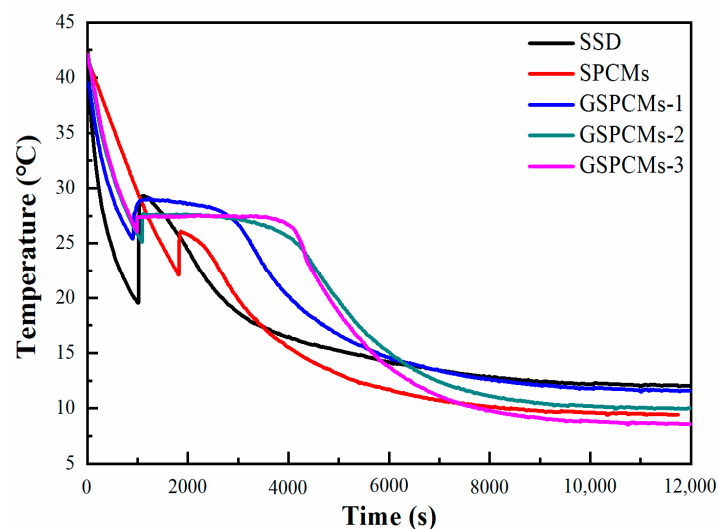


Figure 4. Step cooling curves of the pure $\text{Na}_2\text{SO}_4 \cdot 10\text{H}_2\text{O}$, S-PCMs and GS-PCMs.

3.4. Crystallization Behavior

The XRD patterns of GO, GO- SiO_2 and the GS-PCMs are shown in Figure 5. As can be seen from Figure 5a, a sharp diffraction peak of (002) was observed in GO around $2\theta = 10.4^\circ$, which can be ascribed to the oxygen-containing functional groups contained in the nanosheet structure of GO. The broad diffraction peak at $2\theta = 23.1^\circ$ is a peak characteristic of SiO_2 , indicating the amorphous characteristics of SiO_2 . The diffraction peaks of GO and SiO_2 can be seen for the GO- SiO_2 composites. The crystallization peaks of pure $\text{Na}_2\text{SO}_4 \cdot 10\text{H}_2\text{O}$ and of the composite PCMs are shown in Figure 5b. The diffraction peaks at 19.195° , 23.022° and 25.802° correspond to the crystallization peaks of $\text{Na}_2\text{SO}_4 \cdot 10\text{H}_2\text{O}$. For the S-PCMs that used SiO_2 as a nucleating agent, diffraction peaks of Na_2SO_4 appearing at 23.022° , 39.133° and 60.457° can be observed, while weak diffraction peaks of $\text{Na}_2\text{SO}_4 \cdot 10\text{H}_2\text{O}$ appearing at 19.195° , 23.022° and 25.802° can hardly be detected, indicating the dehydration of $\text{Na}_2\text{SO}_4 \cdot 10\text{H}_2\text{O}$ in the phase change process. The diffraction peaks of $\text{Na}_2\text{SO}_4 \cdot 10\text{H}_2\text{O}$ can be clearly seen from the XRD patterns of the GS-PCMs. It can thus be seen that the incorporation of GO improved the nucleation effect of SiO_2 , resulting in an enhanced crystallization performance for the $\text{Na}_2\text{SO}_4 \cdot 10\text{H}_2\text{O}$ PCMs.

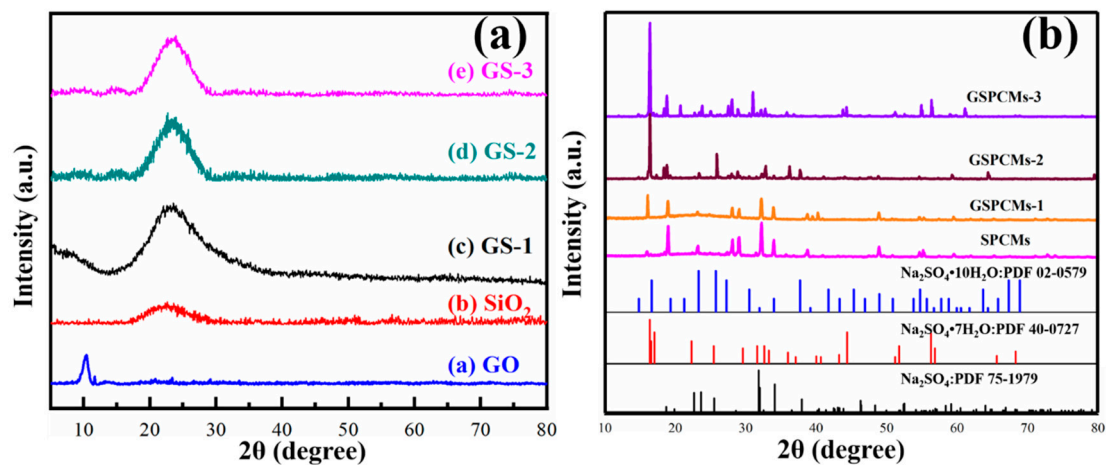


Figure 5. X-ray powder diffractometer (XRD) patterns of (a) GO, SiO₂, GS-1, GS-2 and GS-3; (b) Na₂SO₄·10H₂O, S-PCMs, GS-PCMs-1, GS-PCMs-2 and GS-PCMs-3.

3.5. Phase Change Performance of the Composite PCMs

The phase change performances of the S-PCMs and GS-PCMs were determined using a DSC. The obtained curves in the melting and crystallization process are shown in Figure 6. The phase change performances of Na₂SO₄·10H₂O and of the composite PCMs are shown in Table 2. The melting enthalpy of the pure Na₂SO₄·10H₂O was about 208.2 J/g, with a phase change temperature of about 33.1 °C. The crystallization enthalpy of Na₂SO₄·10H₂O was only about 67.4 J/g, indicating the poor crystallization performance of the pure Na₂SO₄·10H₂O. The addition of SiO₂ and GO–SiO₂ had little influence on the phase change temperature of Na₂SO₄·10H₂O. It can be noted that the crystallization enthalpy of the GS-PCMs obviously increased compared to the pure Na₂SO₄·10H₂O. As the amount of GO in the GO–SiO₂ composites increased, the phase change performance of the Na₂SO₄·10H₂O composite PCMs greatly improved. Among the GO–SiO₂ composite PCMs, GS-PCMs-3 possessed both the highest melting enthalpy, i.e., about 182.7 J/g, and the highest crystallization enthalpy, i.e., about 163.4 J/g.

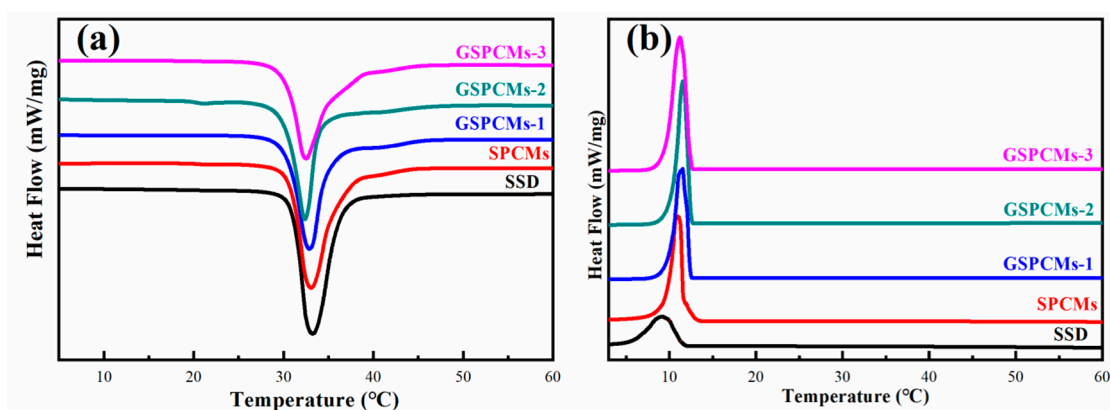


Figure 6. Differential scanning calorimeter (DSC) curves of Na₂SO₄·10H₂O, S-PCMs and GS-PCMs. (a) melting process, (b) cooling process.

Table 2. Phase change performances of the pure $\text{Na}_2\text{SO}_4 \cdot 10\text{H}_2\text{O}$ and composite PCMs.

Sample	Melting		Crystallization	
	Temperature ($^{\circ}\text{C}$)	Melting Enthalpy (J/g)	Temperature ($^{\circ}\text{C}$)	Crystallization Enthalpy (J/g)
$\text{Na}_2\text{SO}_4 \cdot 10\text{H}_2\text{O}$	33.1	208.2	9.4	67.4
S-PCMs	32.8	199.2	10.9	110.8
GS-PCMs-1	32.8	184.5	11.5	138.2
GS-PCMs-2	32.2	168.4	11.2	142.2
GS-PCMs-3	32.5	182.7	11.5	163.4

3.6. Microstructure Analysis of $\text{Na}_2\text{SO}_4 \cdot 10\text{H}_2\text{O}$ Composite PCMs

The microstructures of the $\text{Na}_2\text{SO}_4 \cdot 10\text{H}_2\text{O}$ composite PCMs were tested using SEM. The fine crystalline grains of the pure $\text{Na}_2\text{SO}_4 \cdot 10\text{H}_2\text{O}$ are shown in Figure 7a. As seen from Figure 7b, the addition of SiO_2 resulted in coarse grain particles of $\text{Na}_2\text{SO}_4 \cdot 10\text{H}_2\text{O}$, indicating the weak nucleation effect of SiO_2 that led to the irregular growth of the hydrate salts. Furthermore, to some extent, the change of the grain size also led to the reduction of phase change performance due to the existing phase transition of $\text{Na}_2\text{SO}_4 \cdot 10\text{H}_2\text{O}$ to $\text{Na}_2\text{SO}_4 \cdot 7\text{H}_2\text{O}$ or Na_2SO_4 . In Figure 7c–e, the GS-PCMs with more compact structures can be seen; no coarse grain particles were found in these structures, indicating a better packaging efficiency for GO– SiO_2 composites. It can also be seen that the introduction of GO– SiO_2 refined the grain particle size and improved the crystallization behavior of the hydrate salts. The good compatibility of the hydrophilic GO implied a better combination of SiO_2 with the hydrate salts, which further facilitated the nucleation and crystallization of the $\text{Na}_2\text{SO}_4 \cdot 10\text{H}_2\text{O}$ PCMs [30,31]. The microstructures of the prepared GO– SiO_2 (GS-3) and $\text{Na}_2\text{SO}_4 \cdot 10\text{H}_2\text{O}$ composite PCMs (GS-PCMs-3) were observed by TEM. It can be clearly seen from Figure 8a,b that the spherical SiO_2 nanoparticles were successfully absorbed on the surface of GO, indicating the successful formation of the GO– SiO_2 composites. Figure 8c,d show the successful preparation of GO– $\text{SiO}_2/\text{Na}_2\text{SO}_4 \cdot 10\text{H}_2\text{O}$ composite PCMs; the GO– SiO_2 composite in the $\text{Na}_2\text{SO}_4 \cdot 10\text{H}_2\text{O}$ ensured a better nucleation effect, and the phase change performance of the composite PCMs was also improved.

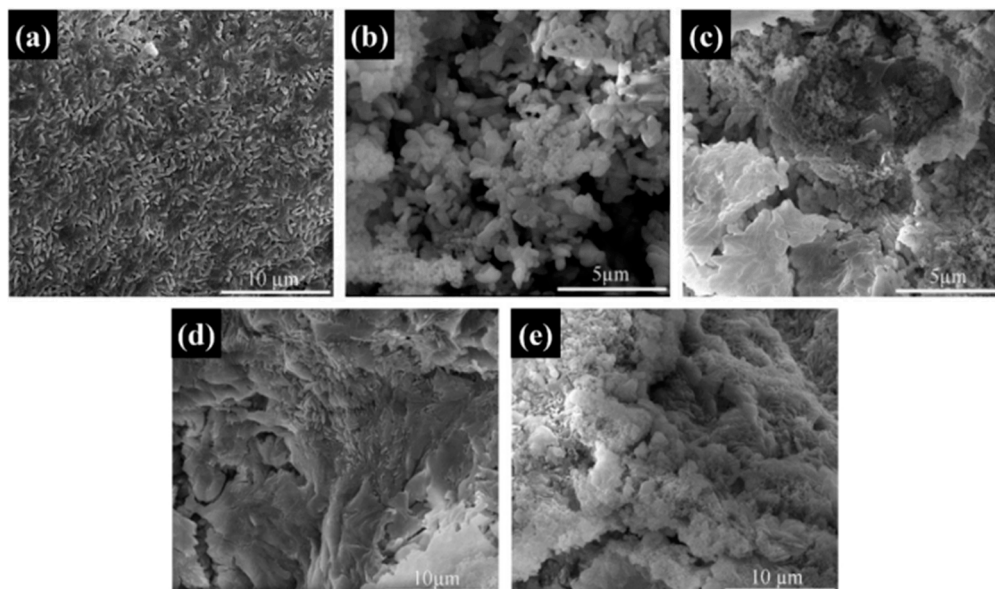


Figure 7. SEM images of (a) pure $\text{Na}_2\text{SO}_4 \cdot 10\text{H}_2\text{O}$, (b) S-PCMs, (c) GS-PCMs-1, (d) GS-PCMs-2, (e) GS-PCMs-3.

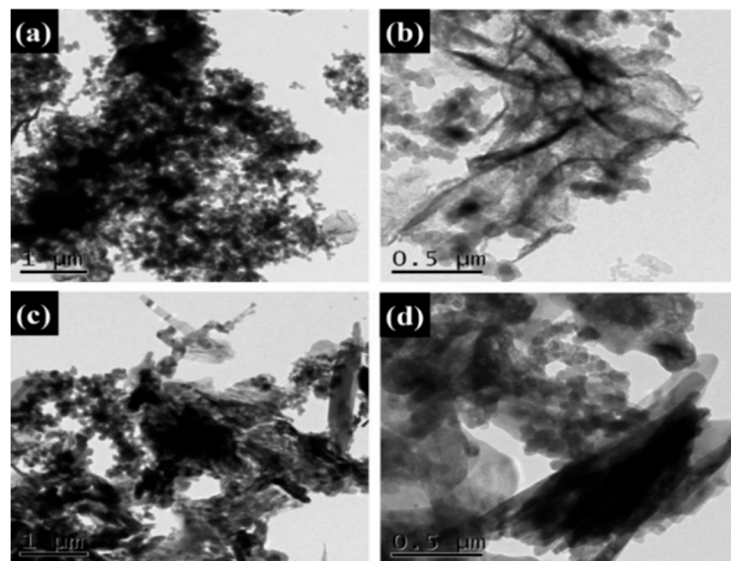


Figure 8. Transmission electron microscopy (TEM) images of (a,b) GO-SiO₂(GS-3) and (c,d) GS-PCMs-3.

3.7. Thermal Conductivity of the Composite PCMs

The thermal conductivity of the prepared S-PCMs and GS-PCMs is shown in Figure 9. The test values of the pure Na₂SO₄·10H₂O, S-PCMs, GS-PCMs-1, GS-PCMs-2 and GS-PCMs-3 were 0.5061 W/(m·K), 0.5419 W/(m·K), 0.5923 W/(m·K), 0.6887 W/(m·K) and 0.6934 W/(m·K), respectively. With the incorporation of GO in the GS-PCMs, the heat transfer performance of the GS-PCMs was enhanced as the specific area of GO-SiO₂. Owing to the incorporation of GO-SiO₂ in Na₂SO₄·10H₂O, the latter was well dispersed and its heat transfer performance enhanced, with higher observed thermal conductivity of the GO-SiO₂ materials. For the prepared sample, the GS-PCMs-3 preserved the highest thermal conductivity, i.e., more than 0.65 W/(m·K), indicating an improvement in the thermal conductivity of the GS-PCMs compared with pure Na₂SO₄·10H₂O.

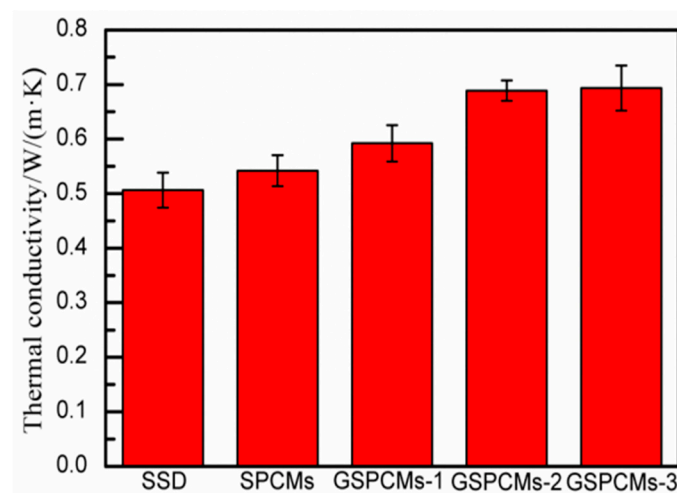


Figure 9. Thermal conductivity of the prepared S-PCMs and GS-PCMs.

4. Conclusions

SiO₂ nanoparticles was prepared and composited with GO to form GO-SiO₂ composite materials with a layered structure. The GO-SiO₂ composites were employed as nucleating agents in the Na₂SO₄·10H₂O PCMs, and the influence of GO on the supercooling degree, crystallization behavior,

phase change performance and thermal conductivity of the $\text{Na}_2\text{SO}_4 \cdot 10\text{H}_2\text{O}$ composite PCMs was investigated. The following conclusions can be drawn:

- (1) Compared to pure SiO_2 , the dispersion performance of the SiO_2 nanoparticles was obviously improved with the introduction of GO, and the specific area of GO- SiO_2 was greatly increased. The high specific area of GO- SiO_2 enabled a good nucleation effect and produced better crystallization behavior for the $\text{Na}_2\text{SO}_4 \cdot 10\text{H}_2\text{O}$ PCMs. In comparison to pure $\text{Na}_2\text{SO}_4 \cdot 10\text{H}_2\text{O}$, the supercooling degree of $\text{Na}_2\text{SO}_4 \cdot 10\text{H}_2\text{O}$ composite PCMs could be reduced from 10.2 to as low as 1.2 °C when 0.45 wt% of GO was added.
- (2) The phase change performance of $\text{Na}_2\text{SO}_4 \cdot 10\text{H}_2\text{O}$ was improved with the incorporation of GO- SiO_2 composites. The crystallization enthalpy of the composite PCMs increased to about 163.4 J/g with the addition of 2.45 wt% of GO- SiO_2 .
- (3) The good compatibility of the hydrophilic GO led to a better combination of SiO_2 with the hydrate salts, which further facilitated the nucleation and crystallization of $\text{Na}_2\text{SO}_4 \cdot 10\text{H}_2\text{O}$. Compared with $\text{Na}_2\text{SO}_4 \cdot 10\text{H}_2\text{O}$, the thermal conductivity of the composite PCMs was improved due to the large specific area of the GO- SiO_2 composites.
- (4) The weight ratio of 2.45 wt% of GO- SiO_2 in the $\text{Na}_2\text{SO}_4 \cdot 10\text{H}_2\text{O}$ was appropriate for achieving a small supercooling degree, high latent heat of the phase change and high thermal conductivity. The prepared GO- SiO_2 composited hydrated salt PCMs demonstrated potential applications in the domain of thermal energy storage materials.

Author Contributions: Conceptualization, Y.Z.; methodology, W.T.; validation, W.T., X.K. and C.F.; formal analysis, W.T. and Y.Z.; investigation, W.T., Y.Z.; X.K.; C.F. and A.B.; data curation, W.T. and Y.Z.; writing—original draft preparation, W.T.; writing—review and editing, W.T. and Y.Z.; project administration, Y.Z.; funding acquisition, Y.Z. All authors have read and agreed to the published version of the manuscript.

Funding: This research was funded by the National Natural Science Foundation of China, grant numbers 51702001 and 51872137, and the Natural Science Foundation of Anhui Province, grant number 1808085QE119.

Conflicts of Interest: The authors declare no conflict of interest.

References

1. Harish, V.S.K.V.; Kumar, A. A review on modeling and simulation of building energy systems. *Renew. Sust. Energy Rev.* **2016**, *56*, 1272–1292. [[CrossRef](#)]
2. Nazir, H.; Batool, M.; Bolivar, O.F.J.; Isaza-Ruiz, M.; Xu, X.; Vignarooban, K.; Phelan, P.; Inamuddin; Kannan, A.M. Recent developments in phase change materials for energy storage applications: A review. *Int. J. Heat. Mass. Tran.* **2019**, *129*, 491–523. [[CrossRef](#)]
3. Kenisarin, M.; Mahkamov, K. Salt hydrates as latent heat storage materials: Thermophysical properties and costs. *Sol. Energy Mater. Sol. Cells* **2016**, *145*, 255–286. [[CrossRef](#)]
4. Fallahi, A.; Guldentops, G.; Tao, M.; Granados, F.S.; Van, D.S. Review on solid-solid phase change materials for thermal energy storage: Molecular structure and thermal properties. *Appl. Therm. Eng.* **2017**, *127*, 1427–1441. [[CrossRef](#)]
5. Lin, Y.; Alva, G.; Fang, G. Review on thermal performances and applications of thermal energy storage systems with inorganic phase change materials. *Energy* **2018**, *165*, 685–708. [[CrossRef](#)]
6. Mariaenrica, F.; Mariateresa, L.; Antonella, S. Phase change materials for energy efficiency in buildings and their use in mortars. *Materials* **2019**, *12*, 1260.
7. Yang, W.; Zhang, L.; Guo, Y.; Jiang, Z.; He, F.; Xie, C.; Fan, J.; Wu, J.; Zhang, K. Novel segregated-structure phase change materials composed of paraffin@graphene microencapsules with high latent heat and thermal conductivity. *J. Mater. Sci.* **2017**, *53*, 2566–2575. [[CrossRef](#)]
8. Khadiran, T.; Hussein, M.Z.; Zainal, Z.; Rusli, R. Advanced energy storage materials for building applications and their thermal performance characterization: A review. *Renew. Sust. Energy Rev.* **2016**, *57*, 916–928. [[CrossRef](#)]

9. Fang, Y.; Su, J.; Fu, W.; Liang, X.; Wang, S.; Gao, X.; Zhang, Z. Preparation and thermal properties of NaOAc·3H₂O·CO(NH₂)₂ non-eutectic binary mixture PCM for radiant floor heating system. *Appl. Therm. Eng.* **2020**, *167*, 114820. [[CrossRef](#)]
10. Zahir, M.H.; Mohamed, S.A.; Saidur, R.; Al-Sulaiman, F.A. Supercooling of phase-change materials and the techniques used to mitigate the phenomenon. *Appl. Energy* **2019**, *240*, 793–817. [[CrossRef](#)]
11. Zhou, S.; Zhou, Y.; Ling, Z.; Zhang, Z.; Fang, X. Modification of expanded graphite and its adsorption for hydrated salt to prepare composite PCMs. *Appl. Therm. Eng.* **2018**, *133*, 446–451. [[CrossRef](#)]
12. Huang, J.; Wang, T.; Zhu, P.; Xiao, J. Preparation, characterization, and thermal properties of the microencapsulation of a hydrated salt as phase change energy storage materials. *Thermochim. Acta* **2013**, *557*, 1–6. [[CrossRef](#)]
13. Dannemand, M.; Johansen, J.B.; Furbo, S. Solidification behavior and thermal conductivity of bulk sodium acetate trihydrate composites with thickening agents and graphite. *Sol. Energy Mater. Sol. Cells* **2016**, *145*, 287–295. [[CrossRef](#)]
14. Zhang, Y.; Zhang, X.; Xu, X.; Muniyalo, J.M.; Liu, L.; Liu, X.; Lu, M.; Zhao, Y. Preparation and characterization of sodium sulfate pentahydrate/sodium pyrophosphate composite phase change energy storage materials. *J. Mol. Liq.* **2019**, *280*, 360–366. [[CrossRef](#)]
15. Shahbaz, K.; AlNashef, I.M.; Lin, R.J.T.; Hashim, M.A.; Mjalli, F.S.; Farid, M.M. A novel calcium chloride hexahydrate-based deep eutectic solvent as a phase change materials. *Sol. Energy Mater. Sol. Cells* **2016**, *155*, 147–154. [[CrossRef](#)]
16. Liu, Y.; Yang, Y. Use of nano- α -Al₂O₃ to improve binary eutectic hydrated salt as phase change material. *Sol. Energy Mater. Sol. Cells* **2017**, *160*, 18–25. [[CrossRef](#)]
17. Xiao, Q.; Yuan, W.; Li, L.; Xu, T. Fabrication and characteristics of composite phase change material based on Ba(OH)₂·8H₂O for thermal energy storage. *Sol. Energy Mater. Sol. Cells* **2018**, *179*, 339–345. [[CrossRef](#)]
18. Liu, C.; Hu, P.; Xu, Z.; Ma, X.; Rao, Z. Experimental investigation on thermal properties of sodium acetate trihydrate based phase change materials for thermal energy storage. *Thermochim. Acta* **2019**, *674*, 28–35. [[CrossRef](#)]
19. Li, X.; Zhou, Y.; Nian, H.; Zhu, F.; Ren, X.; Dong, O.; Hai, C.; Shen, Y.; Zeng, J. Preparation and thermal energy storage studies of CH₃COONa·3H₂O·KCl composites salt system with enhanced phase change performance. *Appl. Therm. Eng.* **2016**, *102*, 708–715. [[CrossRef](#)]
20. Ling, Z.; Liu, J.; Wang, Q.; Lin, W.; Fang, X.; Zhang, Z. MgCl₂·6H₂O·Mg(NO₃)₂·6H₂O eutectic/SiO₂ composite phase change material with improved thermal reliability and enhanced thermal conductivity. *Sol. Energy Mater. Sol. Cells* **2017**, *172*, 195–201. [[CrossRef](#)]
21. Liu, Y.; Yang, Y. Investigation of specific heat and latent heat enhancement in hydrate salt based TiO₂ nanofluid phase change material. *Appl. Therm. Eng.* **2017**, *124*, 533–538. [[CrossRef](#)]
22. Zou, T.; Fu, W.; Liang, X.; Wang, S.; Gao, X.; Zhang, Z.; Fang, Y. Preparation and performance of form-stable TBAB hydrate/SiO₂ composite PCM for cold energy storage. *Int. J. Refrig.* **2019**, *101*, 117–124. [[CrossRef](#)]
23. Peng, S.; Huang, J.; Wang, T.; Zhu, P. Effect of fumed silica additive on supercooling, thermal reliability and thermal stability of Na₂HPO₄·12H₂O as inorganic PCM. *Thermochim. Acta* **2019**, *675*, 1–8. [[CrossRef](#)]
24. Xu, X.; Cui, H.; Memon, S.A.; Yang, H.; Tang, W. Development of novel composite PCM for thermal energy storage using CaCl₂·6H₂O with graphene oxide and SrCl₂·6H₂O. *Energy Build.* **2017**, *156*, 163–172. [[CrossRef](#)]
25. Xia, Y.; Zhang, H.; Huang, P.; Huang, C.; Xu, F.; Zou, Y.; Chu, H.; Yan, E.; Sun, L. Graphene-oxide-induced lamellar structures used to fabricate novel composite solid-solid phase change materials for thermal energy storage. *Chem. Eng. J.* **2019**, *362*, 909–920. [[CrossRef](#)]
26. Li, M.; Wang, W.; Zhang, Z.; He, F.; Yan, S.; Yan, P.J.; Xie, R.; Ju, X.J.; Liu, Z.; Chu, L.Y. Monodisperse Na₂SO₄·10H₂O@SiO₂ microparticles against supercooling and phase separation during phase change for efficient energy storage. *Ind. Eng. Chem. Res.* **2017**, *56*, 3297–3308. [[CrossRef](#)]
27. Yang, S.; Feng, X.; Wang, L.; Tang, K.; Maier, J.; Mullen, K. Graphene-based nanosheets with a sandwich structure. *Angew. Chem. Int. Ed.* **2010**, *49*, 4795–4799. [[CrossRef](#)]
28. Wang, M.; Ma, L.; Shi, L.; Feng, P.; Wang, X.; Zhu, Y.; Wu, G.; Song, G. Chemical grafting of nano-SiO₂ onto graphene oxide via thiol-ene click chemistry and its effect on the interfacial and mechanical properties of GO/epoxy composites. *Compos. Sci. Technol.* **2019**, *182*, 107751. [[CrossRef](#)]

29. Haeri, S.Z.; Ramezanzadeh, B.; Asghari, M. A novel fabrication of a high performance SiO₂-graphene oxide (GO) nanohybrids: Characterization of thermal properties of epoxy nanocomposites filled with SiO₂-GO nanohybrids. *J. Colloid Interface Sci.* **2017**, *493*, 111–122. [[CrossRef](#)]
30. Yang, J.; Tang, L.S.; Bao, R.Y.; Bai, L.; Liu, Z.Y.; Xie, B.H.; Yang, M.B.; Yang, W. Hybrid network structure of boron nitride and graphene oxide in shape-stabilized composite phase change materials with enhanced thermal conductivity and light-to-electric energy conversion capability. *Sol. Energy Mater. Sol. Cells* **2018**, *174*, 56–64. [[CrossRef](#)]
31. Mousavi, A.; Roghani, M.H.; Salami, K.M.; Shahi, S.; Abdollahi, A. Grafting of silica nanoparticles at the surface of graphene for application in novolac-type phenolic resin hybrid composites. *Mater. Chem. Phys.* **2018**, *216*, 468–475. [[CrossRef](#)]

Publisher's Note: MDPI stays neutral with regard to jurisdictional claims in published maps and institutional affiliations.



© 2020 by the authors. Licensee MDPI, Basel, Switzerland. This article is an open access article distributed under the terms and conditions of the Creative Commons Attribution (CC BY) license (<http://creativecommons.org/licenses/by/4.0/>).